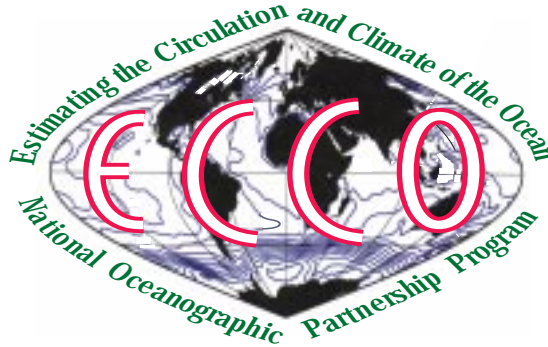


*The ECCO Report Series*¹

Improving ocean angular momentum estimates using a model constrained by data

Rui Ponte, Detlef Stammer and Carl Wunsch

Atmospheric and Environmental Research, Inc., Scripps Institution of
Oceanography, Massachusetts Institute of Technology



Report Number **3**

April, 2000.

¹The ECCO Project is funded through a grant from the National Oceanographic Partnership Program (NOPP). Copies of this Report are available at www.ecco-group.org or from Detlef Stammer, Scripps Institution of Oceanography, La Jolla CA 92093-0230, ph.: (858) 822-3376; fax: (858) 534-4464; e-mail: dstammer@ucsd.edu.

Abstract

Ocean angular momentum (OAM) calculations using forward model runs without any data constraints have recently revealed the effects of OAM variability on the Earth's rotation. Here we use an ocean model and its adjoint to estimate OAM values by constraining the model to available oceanic data. The optimization procedure yields substantial changes in OAM, related to adjustments in both motion and mass fields, as well as in the wind stress torques acting on the ocean. Constrained and unconstrained OAM values are discussed in the context of closing the planet's angular momentum budget. The estimation procedure yields noticeable improvements in the agreement with the observed Earth rotation parameters, particularly at the seasonal timescale. This comparison with Earth rotation measurements provides a stringent independent consistency check on the estimated ocean state and underlines the importance of ocean state estimation for quantitative studies of the variable large-scale oceanic mass and circulation fields, including those on OAM.

1 Introduction

Changes in ocean currents and mass fields imply variability in the ocean angular momentum (OAM) vector, in all its three components: the axial component along the main rotation axis that affect the Earth’s rotation rate or length-of-day (LOD), and two equatorial components that impact on motions of the Earth’s pole of rotation or polar motion (PM). Calculations of OAM were for a long time hampered by the lack of truly global oceanic datasets and models. Only over the last decade have advances in ocean modeling led to the first realistic (non-tidal) OAM estimates [2, 8] and ultimately to the demonstration of the oceans’ role in the excitation of PM [11] and LOD changes [7]. While the success of OAM comparisons with PM and LOD data lend confidence to the quality of the simulations, ocean models are known to have many deficiencies, from poorly parameterized physics to errors in the initial conditions and forcing fields.

To mitigate model shortcomings one can use ocean state estimation methods by which an ocean general circulation model (OGCM) is constrained by large-scale observations (data assimilation), given a priori estimates of the model and data errors. Similar procedures have been applied for many years in numerical weather prediction and the resulting analyses have in fact been used to calculate atmospheric angular momentum (AAM) [13]. In comparison, ocean state estimation is still in its infancy, but its importance for large-scale studies, in combination with increases in computer power and enhanced modeling and data gathering capabilities, have brought this topic now to the forefront of oceanographic research [ECCO and HYCOM Consortia, 2000]. Examples of two global estimation studies now underway can be found in *Stammer et al.* [1997] and *Fukumori et al.* [1999].

Models used in OAM studies thus far are typically forced at the surface by available atmospheric fields, and except for restoring (mostly near-surface) temperature and salinity to observed climatological values, are otherwise not constrained by observations. We report here on a first attempt at estimating OAM based on a constrained ocean model [16]. Our goals are to assess the impact of the state estimation procedure on the OAM values and to examine if the constrained estimates improve the planetary angular momentum budget. While seeking improved OAM values, we also provide a way of checking the efficacy of the estimation procedure in producing better large-scale ocean circulation and mass fields.

2 Estimation of OAM

The OAM vector \mathbf{L} can be written as

$$\mathbf{L} = \mathbf{L}^{\mathbf{P}} + \mathbf{L}^{\mathbf{V}} = \int_V \rho \mathbf{r} \times (\boldsymbol{\Omega} \times \mathbf{r} + \mathbf{v}) dV \quad (1)$$

where ρ and V are the ocean density and volume, and \mathbf{r} , \mathbf{v} , and $\boldsymbol{\Omega}$ represent the position, relative velocity, and Earth’s mean rotation vectors, respectively. The total OAM vector

consists of a matter term \mathbf{L}^P , due to solid body rotation and ultimately related to ocean bottom pressure (p_b) fields, and a motion term \mathbf{L}^V due to velocities relative to the solid body rotation. Following conventional notation [1], the equatorial components of \mathbf{L} are taken along the Greenwich and 90°E meridians and denoted by L_1 and L_2 , respectively, while the axial term is denoted by L_3 . For brevity, expressions for L_1 , L_2 , and L_3 will not be given here; they are easily derived from (1) and can be readily found in the literature [1].

Ponte et al. [1998] and *Ponte and Stammer* [1999, 2000] have used the MIT OGCM described in *Marshall et al.* [1997] in their studies of OAM and its role in the excitation of PM and LOD. The same model is used here. The model is based on the primitive equations under the hydrostatic and Boussinesq approximations. As in previous papers, unmodeled volume changes in the Boussinesq formulation are dealt with by applying a spatially-uniform correction to model sea level so as to conserve total oceanic mass. Current configuration uses 23 vertical levels and 2° horizontal grid spacing on a near-global domain (80°S–80°N). Two sets of OAM values have been calculated for the period 1992–1997. One set is calculated from a run with no data constraints and no optimization. The model is driven by twice-daily wind stress fields and daily heat and freshwater fluxes from the National Centers for Environmental Prediction starting from a spun-up state that is close to *Levitus et al.* [1994] January conditions. A second set of OAM values is obtained from an optimized run in which both initial conditions and surface forcing fields are adjusted so that the model is brought into consistency with a number of global ocean data sets, namely the TOPEX/POSEIDON (T/P) and ERSA-1/2 daily sea surface height (SSH) anomalies and the mean SSH field relative to the EGM-96 geoid model, the *Levitus et al.* monthly mean hydrography, and the *Reynolds and Smith* [1994] sea surface temperature fields. In this run the control vector contained only 10-day averaged forcing fields, thus most of the changes introduced by the optimization are confined to periods > 20 days. See *Stammer et al.* [2000] for details on the model, data sets, and optimization procedure.

Our subsequent analysis focuses on the 5-year period starting on November 1, 1992, to avoid potential problems with transient adjustments to initial conditions and to coincide with start of T/P data set. Figure 1 contrasts the two sets of L_2 values; similar results hold for L_1 and L_3 . The impact of the estimation scheme is clearly seen, with peak-to-peak differences amounting to 50% of the signal. Difference curves are much smoother than the original OAM series, due to the lack of high-frequency changes in the forcing fields. Amplitude of the annual cycle is enhanced. Both L^V and L^P contribute, albeit changes in L^P are larger. Detailed analysis of the implicit changes in p_b and circulation is not possible here, but Figure 2 shows the differences in amplitude of the p_b annual harmonic. The optimization introduces substantial changes in p_b , compared with typical seasonal variability [9], and leads to larger amplitudes in regions like the North Pacific and the Southern Ocean (Pacific sector), which are both important regions for L_2 and also L_1 variability [9]. Changes in the annual cycle of vertically-integrated currents (not shown), on the order of a few mm/s, are also apparent

in most regions.

The changes in OAM are ultimately related to the optimization of the control variables, particularly the wind fields and associated stress torques, and, e.g., some of the changes in L_3 can be readily traced to the zonal stress torque T_z , defined as the area integral of $(r \cos \phi)\tau_z$ where ϕ is latitude and τ_z is zonal stress. As seen in Figure 3, the optimization leads to corrections in the seasonal cycle of T_z on the order of several Hadleys (1 Hadley = 10^{18} kg m²s⁻²) and comparable to typical seasonal variability in T_z [e.g., *Ponte and Rosen*, 1994; Figure 7]. Similar changes are present in L_3 . (The approximate in-phase relation between T_z and L_3 changes at annual period has been explained in terms of the slightly lagged oceanic adjustment to seasonal wind forcing [10].) The suggested large errors in T_z should impact on the axial AAM budget. In fact, comparisons of AAM tendency and torques show substantial imbalances at seasonal timescales, with amplitudes and signs not inconsistent with the results in Figure 3 [*Huang et al.*, 1999; Table 1].

3 Planetary Budget

The atmosphere and the oceans are two major players in the excitation of changes in LOD and PM from seasonal to weekly timescales. Changes in AAM dominate LOD forcing with OAM contributing at the residual level [7, 10]. For PM, and in particular for the annual and Chandler wobbles, OAM effects are as or more important than those of AAM [11, 9]. To assess the impact of the OAM estimation procedure in the context of the solid Earth-atmosphere-ocean angular momentum budget, OAM series are transformed into so-called excitation or χ functions [1], using the relations $(L_1^P, L_2^P) = \Omega(C - A)(\chi_1^P, \chi_2^P)$, $(L_1^V, L_2^V) = \Omega(C - A)(\chi_1^V, \chi_2^V)/1.43$, $(L_3^V, L_3^P) = \Omega C(\chi_3^V, \chi_3^P)/0.70$. Here, C and A are the axial and equatorial moments of inertia of the mantle, respectively, and numerical factors represent elastic Earth effects, as formulated using Love numbers. Values of $C = 7.04 \times 10^{37}$ kg m² and $C - A = 0.00333C$ are used here [1]. The functions χ are non-dimensional and represent effective excitation of LOD and PM given OAM and AAM time series. Equivalent observed excitation functions can be derived from the geodetic determination of the Earth's orientation in space. In the present analysis, the atmospheric and geodetic excitation functions, hereafter denoted by superscripts A and G , respectively, are the ones described in detail by *Ponte and Stammer* [1999, 2000].

Focusing on the terms relevant for PM, Figure 4 shows the annual and semiannual wobble excitation budget computed using standard Fourier decomposition. With only five years of records, a stable estimate of mean seasonal conditions is not expected. (Separation of the Chandler excitation at ~ 14 months from the large annual cycle is also difficult and thus not attempted here.) Instead, our purpose is to examine the impact of ocean data assimilation on estimates of OAM. A comparison with Figure 4 of *Ponte and Stammer* [1999], which is based on the 11-year record 1985–1995, provides a measure of the variability expected

from using different periods and confirms the interannual modulation of the seasonal OAM signals noted in the earlier study. Results in Figure 4 based on the two different OAM values show large differences, particularly for the annual period: the assimilation leads to a large increase in the amplitude of χ_2 and a noticeable phase shift in χ_1 , providing for substantially improved budget on the annual period. And, although weaker, the impact of the data assimilation likewise leads to reduced residuals on semiannual terms as well.

Coherence amplitudes between χ^G and χ^A and χ^{A+O} at sub-seasonal periods are shown in Figure 5. Results confirm the positive impact of adding OAM to AAM excitation, down to periods of ~ 5 days [11, 6]. More important in the present context is that constrained OAM values provide slightly higher coherence amplitudes at periods > 30 days. For the periods ranging from annual to 20 days, time series of χ^{A+O} based on constrained OAM estimates can explain 71% and 74% of the variance in χ_1^G and χ_2^G , respectively, compared to only 66% and 65% for unconstrained estimates. (Explained variance is calculated as $[\text{var}\{\chi^G\} - \text{var}\{\chi^G - \chi^{A+O}\}]/\text{var}\{\chi^G\}$.) Most of these gains come from the changes in the annual cycle of L_1 and L_2 (Figure 4).

For the LOD budget, the impact of optimization is minor. The largest change occurs at the annual cycle (Figure 3), with constrained estimates having twice the amplitude and a phase which is shifted by more than 2 months relative to the unconstrained run. These differences lead to better agreement with the residual $\chi_3^G - \chi_3^A$ (Figure 6), but we note that uncertainties in the latter residual are also substantial [8, 10]. In fact, the minor impact of the assimilation at sub-seasonal periods indicates that the potential improvements on OAM might be within the noise level of current LOD budgets.

4 Summary

Analysis of OAM quantities calculated from output of a global model constrained by data (altimetry, monthly hydrography, and sea surface temperature) reveals a clear impact of the optimization procedure on the large scale (vertically averaged) circulation and mass fields. All three OAM components are substantially changed, particularly at seasonal timescales, providing for better agreement with observed signals in LOD and PM. The comparison with Earth rotation data attests to the beneficial impact of the estimation scheme on OAM values and constitutes a novel consistency check on the estimated oceanic large scale fields. The optimization also yields substantial adjustments to the seasonal wind stress fields, which can be checked in the context of the AAM budget.

Because ocean state estimation is still in its infancy, our results should be considered as preliminary. In particular, there seems to be important information in the data at high frequencies which was not used yet because the control vector was limited to 10-day averaged forcing fields. Issues of interest for future investigation include whether the benefits of optimization can be extended to periods < 20 days, and whether the implicit surface wind

torque corrections can improve the AAM budget. With expected improvements in model resolution and parameterizations, more data collection, and better estimation methodologies, calculation of seasonal to daily OAM signals with accuracies approaching those of AAM estimates should become possible in the near future, making feasible at the same time the investigation of other geophysical signals in LOD and PM that are currently in the noise level.

Acknowledgments

R.P. gratefully acknowledges the support of the NASA Solid Earth and Natural Hazards Program (contracts NAS5-97270 and NAS5-98182). D.S. was supported by contract JPL-68571, by contract NAGW-7857 with NASA, and through ONR (NOPP) grant N00014-99-1-1049. C.W. was supported by the ECCO (NOPP) Consortium under ONR Grant N00014-99-1-1050.

References

- [1] Barnes, R. T. H., R. Hide, A. A. White, and C. A. Wilson, Atmospheric angular momentum fluctuations, length-of-day changes and polar motion. *Proc. R. Soc. London, Ser. A*, *387*, 31–73, 1983.
- [2] Brosche, P., J. Wunsch, A. Frische, J. Sündermann, E. Maier-Reimer, and U. Mikolajewicz, The seasonal variation of the angular momentum of the oceans, *Naturwissenschaften*, *77*, 185–186, 1990.
- [3] Fukumori, I., R. Raghunath, L.-L. Fu, and Y. Chao, Assimilation of TOPEX/Poseidon altimeter data into a global ocean circulation model: How good are the results?, *J. Geophys. Res.*, *104*, 25,647–25,665, 1999.
- [4] Huang, H.-P., P. D. Sardeshmukh, and K. M. Weickmann, The balance of global angular momentum in a long-term atmospheric data set, *J. Geophys. Res.*, *104*, 2031–2040, 1999.
- [5] Levitus, S., R. Burgett, and T. Boyer, *World Ocean Atlas 1994*, vol. 3, *Salinity*, and vol. 4, *Temperature*, *NOAA Atlas NESDIS 3 & 4*, U.S. Dep. of Comm., Washington, D.C., 1994.
- [6] Nastula, J., and R.M. Ponte, Further evidence for oceanic excitation of polar motion, *Geophys. J. Int.*, *139*, 123–130, 1999.
- [7] Marcus, S. L., Y. Chao, J. O. Dickey, and P. Gegout, Detection and modeling of nontidal oceanic effects on Earth’s rotation rate, *Science*, *281*, 1656–1659, 1998.

- [8] Ponte, R. M., and R. D. Rosen, Oceanic angular momentum and torques in a general circulation model, *J. Phys. Oceanogr.*, *24*, 1966–1977, 1994.
- [9] Ponte, R. M., and D. Stammer, Role of ocean currents and bottom pressure variability on seasonal polar motion, *J. Geophys. Res.*, *104*, 23,393–23,409, 1999.
- [10] Ponte, R. M., and D. Stammer, Global and regional axial ocean angular momentum signals and length-of-day variations (1985–1996), *J. Geophys. Res.*, accepted, 2000.
- [11] Ponte, R. M., D. Stammer, and J. Marshall, Oceanic signals in observed motions of the Earth’s pole of rotation, *Nature*, *391*, 476–479, 1998.
- [12] Reynolds, R. W., and T. M. Smith, Improved global sea surface temperature analysis using optimum interpolation, *J. Clim.*, *7*, 929–948, 1994.
- [13] Salstein, D. A., D. M. Kann, A. J. Miller, and R. D. Rosen, The sub-bureau for atmospheric angular momentum of the international earth rotation service: a meteorological data center with geodetic applications, *Bull. Amer. Meteor. Soc.*, *74*, 67–80, 1993.
- [14] Stammer, D., C. Wunsch, R. Giering, Q. Zhang, J. Marotzke, J. Marshall, and C.N. Hill, The global ocean circulation estimated from TOPEX/POSEIDON altimetry and the MIT general circulation model. *MIT Center of Global Change Science, Report 49*, 1997.
- [15] Stammer, D., and E. Chassignet, The, Ocean State Estimation and Prediction in Support of Oceanographic Research, submitted for publication, 2000.
- [16] Stammer, D., C. Wunsch, R. Giering, C. Eckert, P. Heimbach, J. Marotzke, A. Adcroft, C.N. Hill, and J. Marshall, The global ocean circulation and transports during 1992–1997, estimated from ocean observations and a general circulation model, in preparation, 2000.

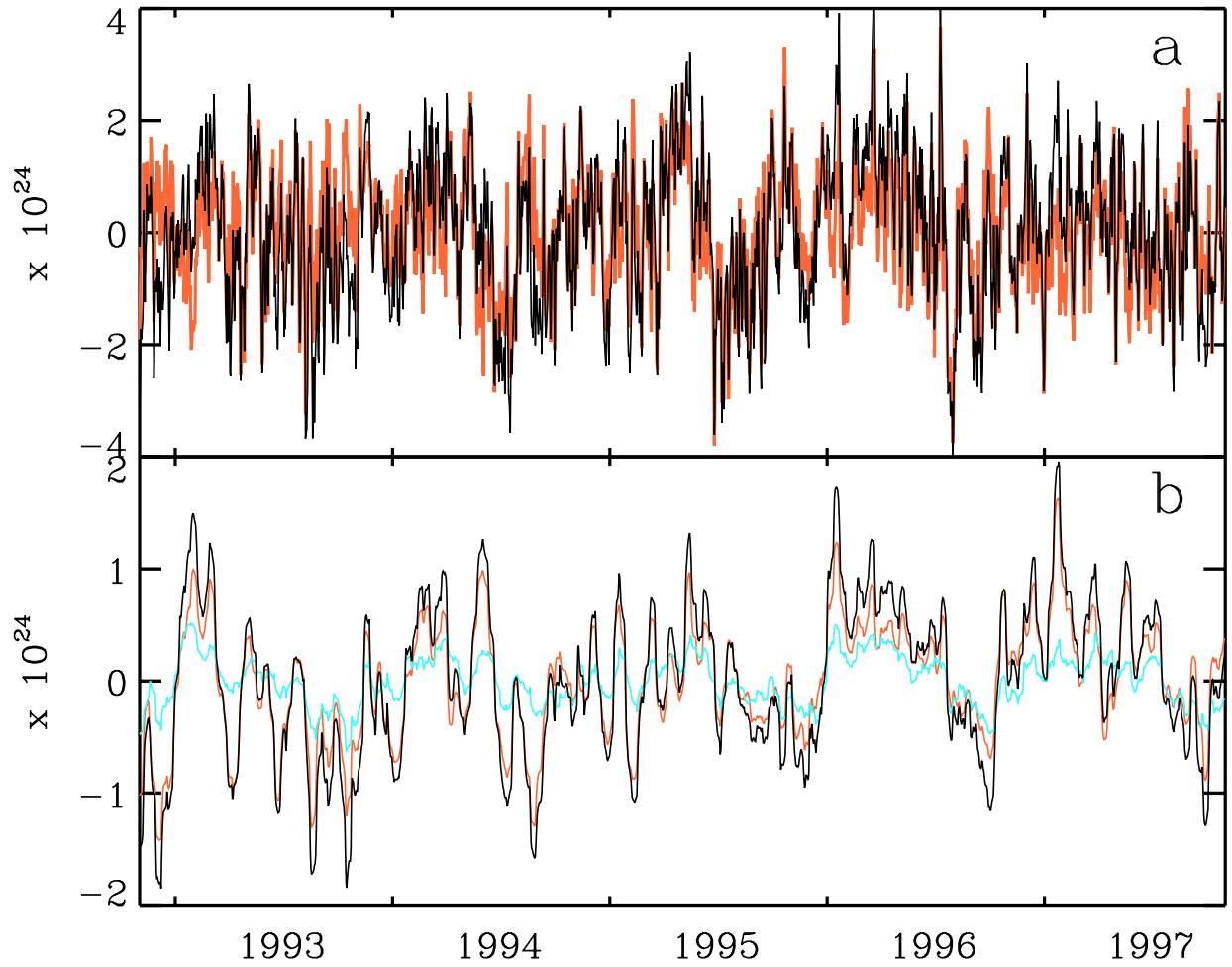


Figure 1: (a) Time series of L_2 in $\text{kg m}^2 \text{s}^{-1}$, starting in November 1, 1992. Unconstrained values are in red, constrained values in black. (b) Constrained minus unconstrained values for L_2 (black), L_2^P (red), and L_2^V (blue).

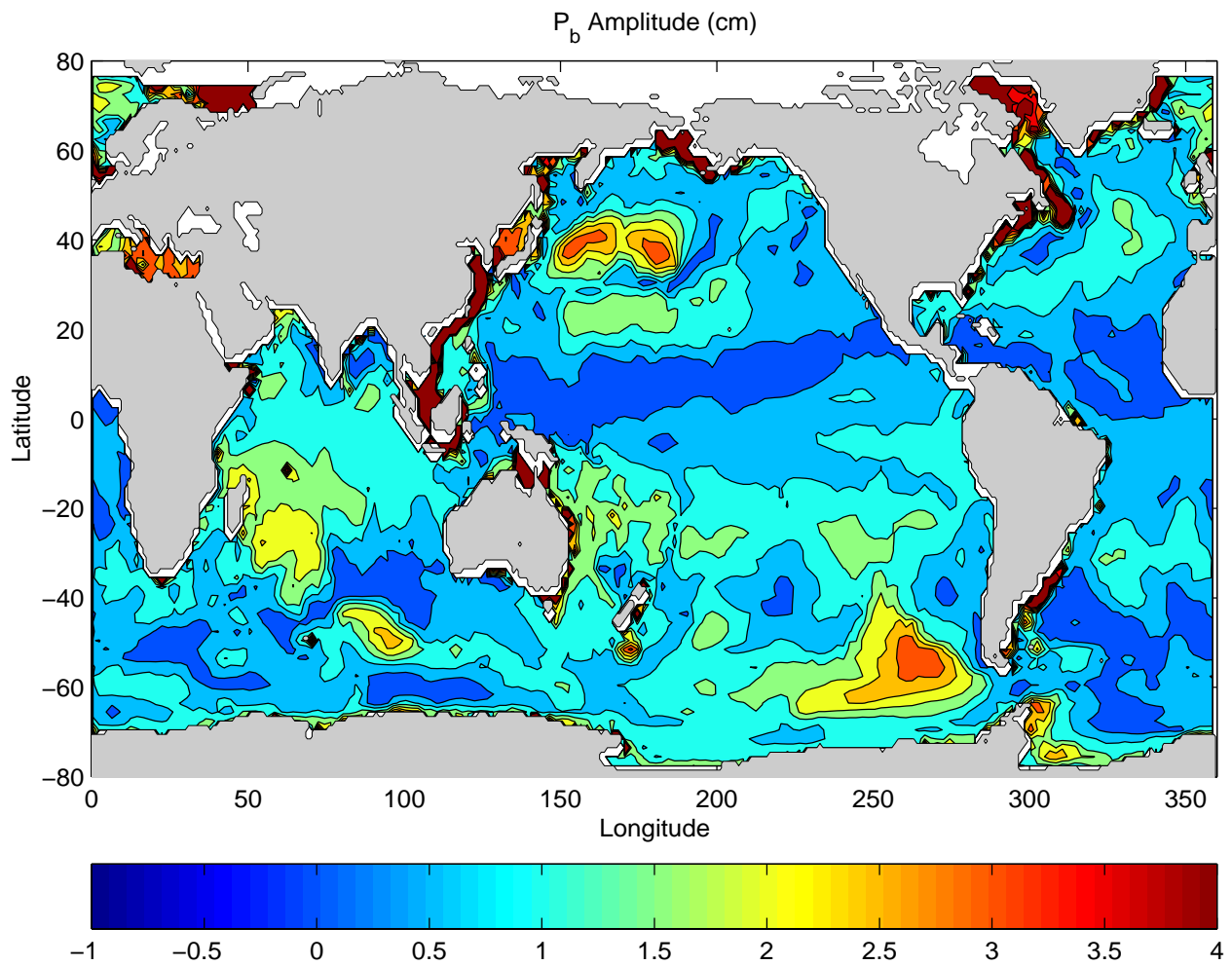


Figure 2: Constrained annual cycle amplitudes of bottom pressure p_b minus unconstrained values (in equivalent centimeters of water).

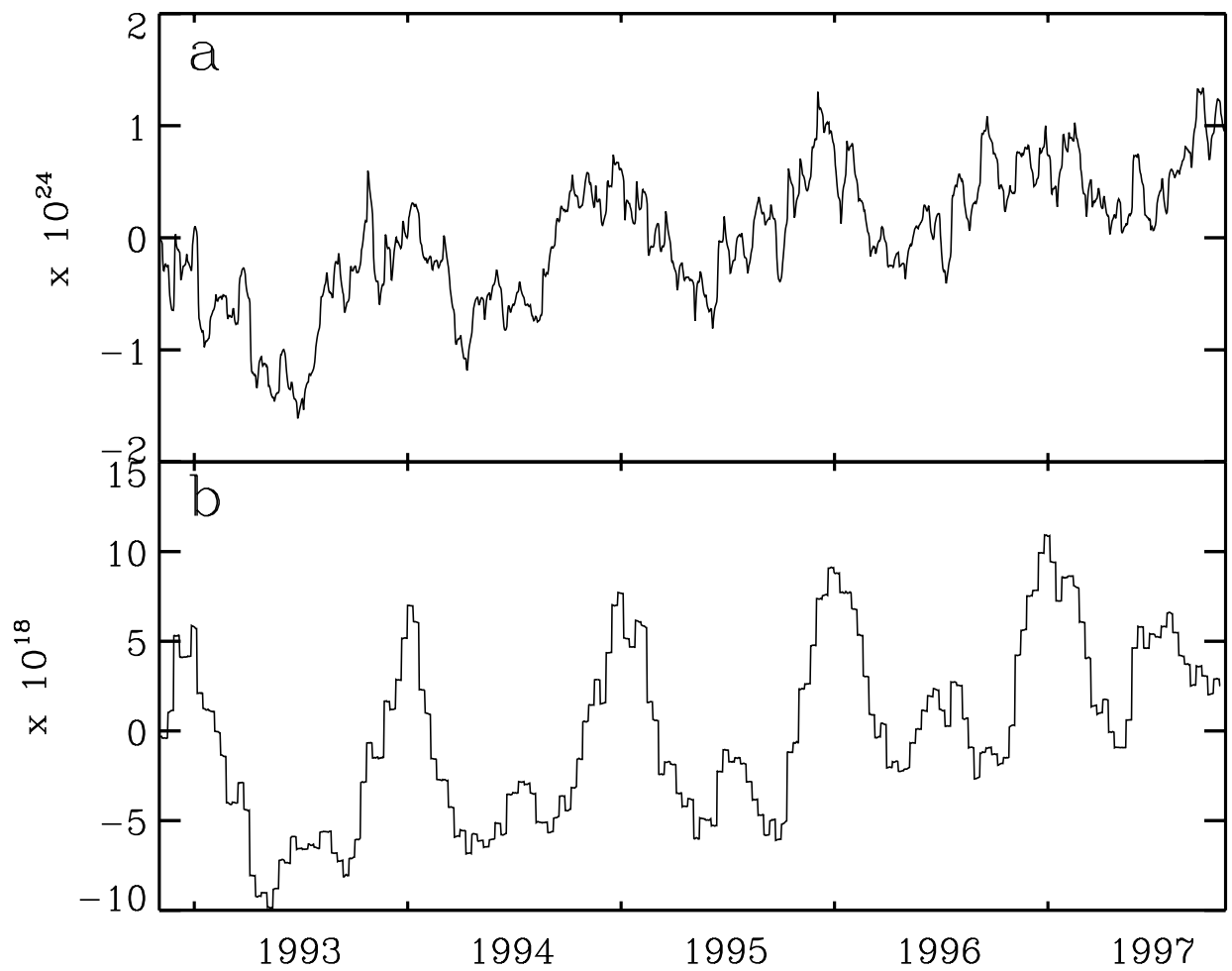


Figure 3: Constrained minus unconstrained values of (a) L_3 in $\text{kg m}^2 \text{s}^{-1}$ and (b) zonal wind stress torque over the ocean T_z in $\text{kg m}^2 \text{s}^{-2}$.

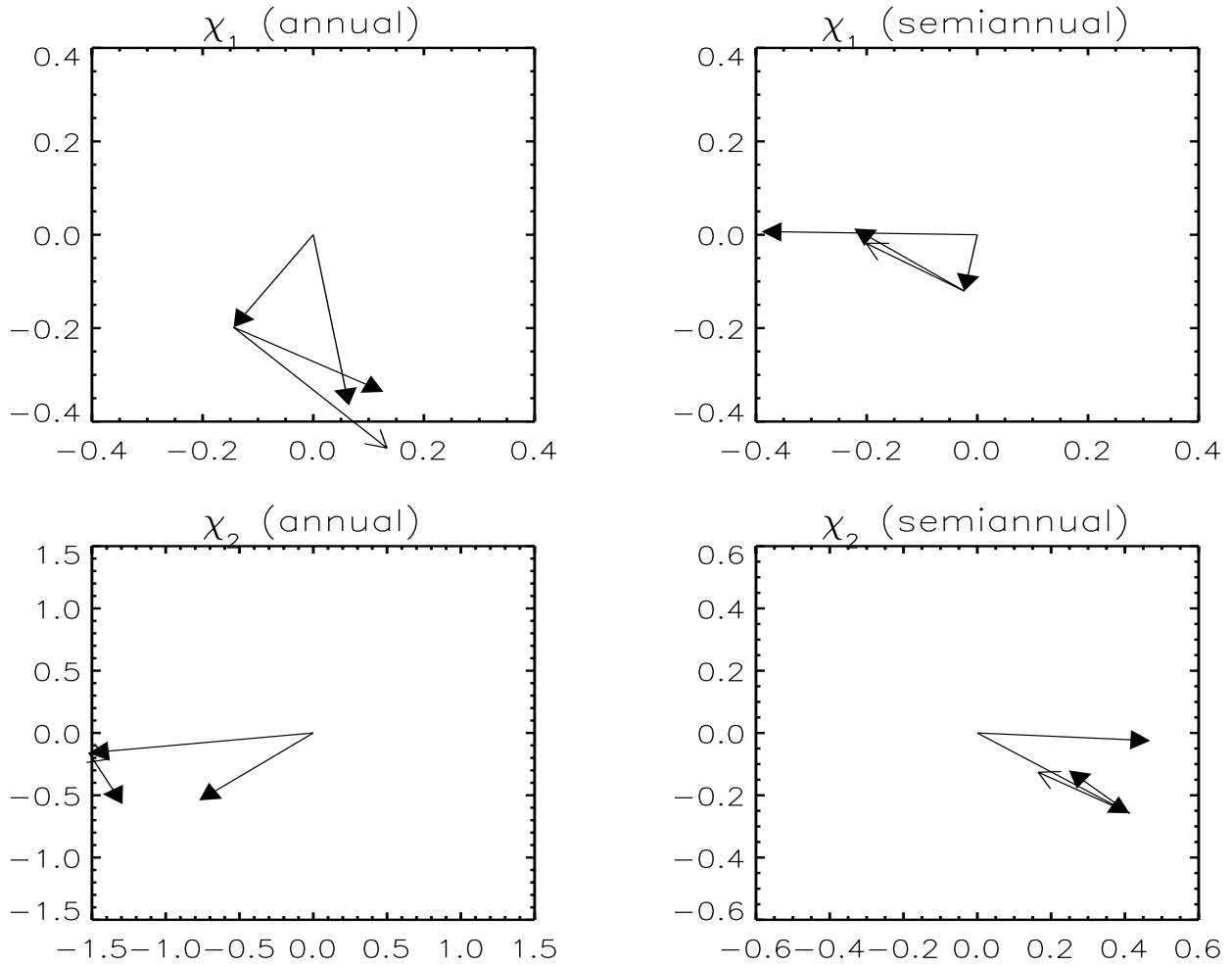


Figure 4: Phasor diagram for annual and semiannual wobble excitation in χ_1 (top) and χ_2 (bottom). Vectors represent dimensionless amplitudes ($\times 10^{-7}$) and phases of χ^G , χ^A , and χ^O . An arrow pointing due east (south) denotes a maximum on \sim January 1 (April 1). χ^G and χ^A vectors share the origin, and χ^O is added to χ^A . Solid arrows denote constrained χ^O values.

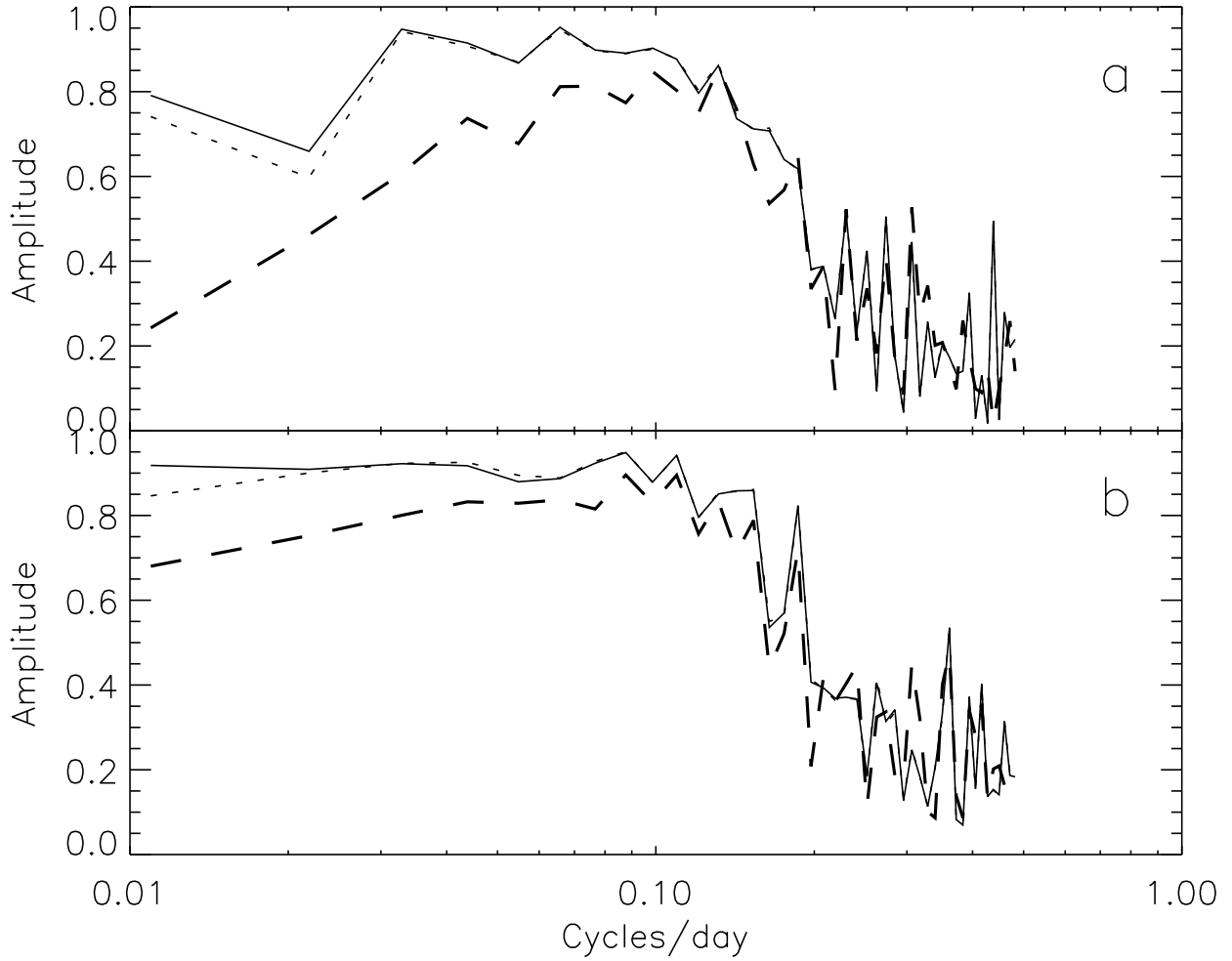


Figure 5: Coherence amplitude between χ_1^G and χ_1^A (dashed), unconstrained χ_1^{O+A} (dotted), and constrained χ_1^{O+A} (solid), calculated with band-averaging over 20 frequencies. First point plotted represents the 6–2 month band. Coherence amplitudes larger than 0.38 are significantly different from zero at the 95% confidence level. (b) As in (a) but for χ_2 quantities.

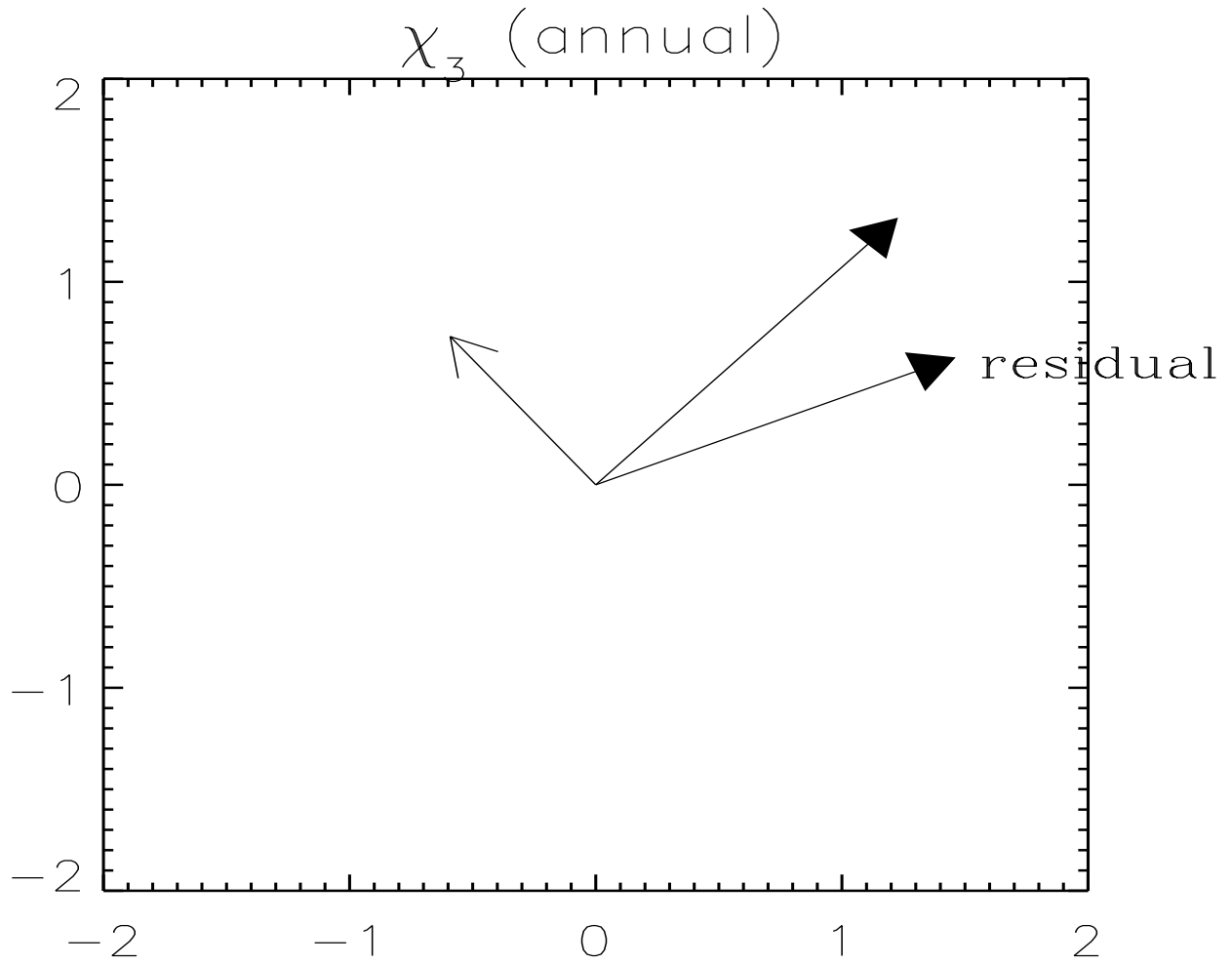


Figure 6: Phasor diagram for annual excitation in χ_3 . Vectors represent dimensionless amplitudes ($\times 10^{-9}$) and phases of $\chi^G - \chi^A$ (residual curve) and χ^O . Solid arrow denotes constrained χ^O value. Phase is plotted as in Figure 4.